Article

Study on Properties of Micro-Nano Magnetic Composite Prepared by Mechanochemical Method of *NdFeB* Secondary Waste and Removal of As (V) from Mine Water

Xiujuan Feng [1,2,3,4,*] and Yicheng Rao [1,3,4]

1   School of Mines, China University of Mining and Technology, Xuzhou 221116, China
2   Ji'an Xintai Technology Co., Ltd., No. 6, Fengming Avenue, Ji'an Hi-Tech Industrial Development Zone, Ji'an County, Ji'an 343100, China
3   School of Information and Control Engineering, China University of Mining and Technology, Xuzhou 221116, China
4   Mechano Chemistry Research Institute, China University of Mining and Technology, Xuzhou 221116, China
*   Correspondence: xjfeng@cumt.edu.cn

Abstract: The secondary waste produced by *NdFeB* waste after rare earth recycling, with an annual output of more than tens of thousands of tons, is the largest solid waste emission source in the rare earth industry, and long-term storage causes land resource occupation and environmental pollution. Arsenic-containing mine wastewater has serious harm, wide distribution, and long duration of pollution. In this study, the mechanical ball milling method was used to activate NdFeB secondary waste to prepare micro-nano magnetic composite materials, the main components of which are Fe_2O_3, Fe_3O_4, and C. Under mechanical mechanochemical action, the particles are more dispersed, the particle size decreases, the specific surface area increases significantly, the crystal structure changes to amorphous structure, the degree of amorphous shape increases, and the content of Fe-OH increases. Applied to the treatment of As (V) in simulated mine water, it was found that the removal of As (V) by this material was mainly based on chemisorption and monolayer adsorption, and the maximum adsorption amount reached 10.477 mg/g. Zeta, FT-IT, and XPS characterization confirmed that the removal of As (V) was a coordination exchange reaction between the material and As (V) to form an inner sphere complex. The removal rate of As (V) decreased from 94.33% to 73.56% when the initial concentration of solution was 10 mg/L, pH value was 3.0, and material dosage was 1 g/L after 5 times of regrowth. This study provides a new way for the application of NdFeB secondary waste, which has low cost, green environmental protection, and wide application prospects.

Keywords: high-energy ball milling; mechanochemistry; *NdFeB* Secondary Waste; micro and nano magnetic composites; mine water; As (V)

1. Introduction

NdFeB waste is the solid waste generated by NdFeB permanent magnet materials in the process of cutting, grinding, and polishing, accounting for about 30% of the total raw materials for magnet production [1]. China is a major producer of NdFeB permanent magnet materials. From 2002 to 2021, the production of NdFeB permanent magnet materials increased from 62,000 tons to 213,300 tons [2]. The NdFeB waste generated in the production process also increases year by year and is expected to produce 27,000–54,000 tons of NdFeB waste in 2030 [3]. NdFeB waste contains 27–33% rare earth elements and 66–73% iron elements, which have high recycling value [4]. If it is directly discharged into the environment, it is easy to cause heavy metal pollution and waste of resources [5]. At present, the hydrochloric acid optimal solution method, total solution method, and double salt precipitation method are used to recover and treat rare earth elements in NdFeB waste [6]. NdFeB secondary waste is the solid waste produced by NdFeB waste after rare

earth recycling and treatment. Its main components are iron oxide and graphite, with an annual output of more than tens of thousands of tons, and it is one of the largest solid waste discharge sources for rare earth enterprises. Long-term storage is easy to cause land resource occupation and environmental pollution [7].

The mechanical mechanochemical method, also known as ball milling method, is a green and efficient modification method. The principle of mechanical force is to grind, compress, shear, and impact the ball milling material so that the physical and chemical properties of the material are changed, the crystal structure is destroyed, and the surface properties are changed to improve the adsorption properties of the material [8]. The mechanochemical method is widely used in the fields of material surface modification and synthesis [9], heavy metal separation [10], and solid waste recycling [11] due to its advantages of simple operation, easy control of reaction process, and more green environmental protection without adding other chemical reagents. Haowen Zou et al. [12] successfully prepared a new biochar/iron oxide composite material (BM-Fe-HC) for Cr(VI) wastewater treatment by placing Fe-HC in a planetary ball mill at a ball milling speed of 500 r/min for 4 h. The experimental results showed that ball milling effectively reduced the particle size, increased the specific surface area, and exposed more iron oxide to the surface of biochar, which was beneficial to the adsorption of Cr(VI). The maximum adsorption capacity reached 48.1 mg/g, which was much higher than that of other biochar/iron complexes. Fang Li et al. [13] successfully prepared a new adsorbent for the treatment of wastewater containing As (V) by ball-milling 20% pecan biochar and 80% expanded vermiculite. The test results showed that under the mechanochemical action, the specific surface area, pore volume, and surface functional group increased significantly, the crystallinity of the material changed significantly, and the material had stronger adsorption capacity than the raw material.

The mining of mine resources has caused many environmental problems. For example, mining exposes buried metal sulfide minerals to the surface and forms acid mine wastewater (AMD) after oxidation by air and microorganisms and erosion by rain [14]. Arsenic (As) is one of the main ore-forming elements of sulfide minerals. According to statistics, every 1 t of gold extracted in China will be accompanied by 1732 to 20,829 t of arsenic, and every 1 t of other metals except gold will be accompanied by 0.12 to 10.8 t of arsenic [15]. Arsenic mainly exists in AMD is arsenate (As V) with the oxidation and dissolution of sulfide minerals [16], and with the flow of AMD contaminating surrounding rivers and groundwater, it infiltrates into farmland, resulting in excessive arsenic content in water and soil [15]. For example, the wastewater from the Richmond iron mine in the United States contains as much as 850 mg/L of arsenic [17]. The Ottery mine in Australia ceased operation in 1936, but the river around the mine was still found to contain as much as 10 mg/L of arsenic [18]. The maximum arsenic content of rivers in the Dabaoshan mining area in China is as high as 175 µg/L [19], and many mining areas in Hunan, Guizhou, and Inner Mongolia are faced with different degrees of AMD arsenic pollution [20,21]. Therefore, the treatment of arsenic in mine water is imperative.

Currently, the main methods for removing As (V) from the aquatic environment include ion exchange, bioremediation, chemical precipitation, membrane separation, and adsorption. The ion exchange method can extract harmful ions from polluted water, which has the advantages of rapid reaction, high removal efficiency and being renewable [22]. However, this method is cumbersome and requires filtration prior to use to eliminate organic compounds that may damage the resin. In addition, other coexisting anions in the water body will form a competitive relationship with arsenate ions, greatly reducing the removal rate of arsenate ions and accelerating the consumption of exchangers [23]. The bioremediation method requires only a small amount of nutrient inputs for investment, which is inexpensive and has the advantages of being easy to manage and green [24]. However, the plant growth cycle is long and the efficiency of arsenic treatment is low [25]. The chemical precipitation method is simple and suitable for large-scale treatment of arsenic-containing wastewater. However, the arsenic-containing chemical precipitates formed after

the reaction are difficult to remove, creating a new solid waste pollution problem. Although the membrane separation method has a better arsenic removal effect, due to the high cost of the membrane, the treatment process requires high energy consumption [26]. Therefore, the membrane separation method is difficult to be widely used in practical arsenic-containing wastewater treatment.

In arsenic removal formula technology, the adsorption method is widely used because of its good removal effect, simple operation, and rapid reaction [27].

Therefore, this paper uses mechanical force to activate NdFeB secondary waste to prepare magnetic micro-nano composite for mine As (V) wastewater treatment, providing a new idea for comprehensive utilization of NdFeB secondary waste.

2. Materials and Methods

2.1. Chemicals and Material

(1) Reagents

Sodium arsenate dodecahydrate ($Na_3AsO_4 \cdot 12H_2O$), hydrochloric acid (HCl), sodium hydroxide (NaOH), sodium chloride (NaCl), anhydrous sodium sulfate (Na_2SO_4), chromium chloride ($CdCl_2$), anhydrous calcium chloride ($CaCl_2$), and magnesium chloride hexahydrate ($MgCl_2 \cdot 6H_2O$) were all purchased from Sinopharm Group Reagent Co., Ltd (Shanghai, China).

(2) Source and composition of raw materials

The NdFeB secondary waste comes from Ji'an Co., Ltd., Jiangxi Province (Ji'an, China), and its main components are shown in Table 1.

Table 1. Content of various elements in neodymium iron boron secondary waste.

Elements	Wt/%	At/%
O	51.9	0.5
C	24.7	0.6
Fe	23.4	0.3

According to the analysis of Table 1, NdFeB secondary waste mainly consists of Fe, O, and C elements.

(3) Simulate wastewater containing As (V)

A total of 5.658 g of $Na_3AsO_4 \cdot 12H_2O$ was accurately weighed into a 1 L volumetric flask, and then added with deionized water to the scale, shaken well to obtain 1 g/L As (V) stock solution, which was protected from light. The As (V) solution used in the subsequent tests was prepared by diluting 1 g/L As (V) stock solution.

2.2. Magnetic Micro-Nano Composite Materials Preparation

The NdFeB secondary waste is placed in the oven at 105 °C for 24 h and then taken out after drying, ground through a 50-mesh sieve, and stored for later use. The NdFeB secondary waste that has been dried for 50 mesh screens is taken as the raw material, and 5 g of raw material is placed in the model QXQM-2 (Changsha, China) planetary ball mill. The ball grinding parameters are set as the grinding time of 150 min, the grinding speed of 400 r/min, and the ball material ratio of 10:1. After the ball grinding, the material is put in the sample bag, sealed, and stored. The preparation process of micro- and nano-magnetic composites is shown in Figure 1.

Figure 1. Process flowchart for preparing micro-nano magnetic composite materials.

2.3. Characterization

Quatto S field emission scanning electron microscopy (SEM-EDS), produced by the FEI Company of Czech Republic (Karlsruhe, Germany), was used to observe the changes in the micromorphology of the materials before and after mechanochemical activation and adsorption of As (V), and the composition and content of the surface elements were analyzed. The D8 Advance X type X-ray diffractometer (XRD) produced by Bruck AXS Co., Ltd. (Karlsruhe, Germany). in Germany was used to measure the materials before and after mechanochemical activation, and the composition of the raw materials and the crystal structure changes of the materials before and after mechanochemical action were analyzed. The test conditions were Cu target (Kα radiation), and the working voltage was 40 KV. The current is 100 mA, the scanning range is 10–80°, and the scanning speed is 2°/min. The TENSORII Fourier infrared spectrometer (FFT-IR) produced by Bruker Spectroscopy of Germany (Karlsruhe, Germany) was used to test the materials before and after the mechanical chemical action and the adsorption of As (V). The test wave number range was 500–4000 cm^{-1}, the resolution was 1.0 cm^{-1}, and the scanning times were 33. The ESCALab250Xi X-ray photoelectron spectrometer (XPS) produced by Thermo Scientific in the United States (Waltham, MA, USA) was selected to conduct broad spectrum scanning of the samples before and after adsorption of As (V), and the four elements C, Fe, O, and As were narrowly scanned. The test results were corrected with C1s binding energy (284.8 volts) as reference. The test results of XPS elements were fitted using Avantage software (v5.9921). Zetasizer Nano ZSE potential and nano-particle size analyzer produced by Malvern Instruments Co., Ltd. (Malvern, England). were used to test the Zeta potential of the material before and after adsorption As (V) at different pH values (1, 3, 5, 7, 9, 11).

2.4. Batch Sorption

(1) Comparison of NdFeB secondary waste vs. micro-nano composite removal of As (V)

Weighing 0.05 g of NdFeB secondary waste and micro- and nano-magnetic composites, the mixture was placed in a 200 mL conical flask, 50 mL of As (V) solution at a concentration of 10 mg/L was added, and the pH of the mixture was adjusted to 3.0 by dropping in 0.1 mol/L hydrochloric acid. The mixture was placed in a water-bath thermostatic oscillator at a reaction temperature of 25 °C and a rotational speed of 160 r/min, and the reaction was carried out by shaking the reaction using samples that were taken at different reaction times (0, 5, 10, 20, 30, 60, 90, 120 min) by syringe, filtered through 0.45 μm aqueous filter membrane, and the concentration of the filtrate was determined by ICP-OES.

(2) Test on the effect of initial pH of solution on the removal rate of As (V)

Weigh 0.05 g magnetic micro-nano composite material, place it in 200 mL conical bottle, and add 50 mL of As (V) solution with a concentration of 10 mg/L, add 0.1 mol/L of hydrochloric acid or 0.1 mol/L sodium hydroxide to adjust the mixture to different pH values (1.0, 3.0, 5.0, 7.0, 9.0, and 11.0). The mixture was placed in a water bath thermostatic oscillator at a reaction temperature of 25 °C and a rotating speed of 160 r/min for 120 min, and then sampled, filtered by 0.45 μm water filter membrane, and the concentration of filtrate was determined by ICP-OES.

(3) Test on the influence of coexisting ions on As (V) removal rate

Using 10 mg/L of As (V) solution as the base solution, use $CdCl_2$, $MgCl_2 \cdot 6H_2O$, $CaCl_2$, NaCl, and Na_2SO_4 to prepare the coexistence of Cd^{2+}, Mg^{2+}, Ca^{2+}, Cl^-, and SO_4^{2-} with different ion concentrations (1, 10, 100 mM).Take 200 mL conical bottle, add 50 mL mixed solution of different concentrations and co-existing ions, drop 0.1 mol/L hydrochloric acid into it to adjust its pH to 3.0. Weigh 0.05g (prepared under optimal conditions) magnetic micro-nano composite material and add it into the mixed solution. The conical bottle was placed in a water bath thermostatic oscillator, the water bath temperature was 25 °C, the rotating speed was 160 r/min, and the oscillation reaction was 120 min. The reaction solution was filtered by 0.45μm aqueous filter membrane, and the filtrate concentration was analyzed by ICP-OES.

(4) Repeated material regeneration test

Weigh 0.05 g of magnetic micro-nano composite material, put it into a 200 mL conical bottle, add 50 mL of As (V) solution with a concentration of 10 mg/L, drop it into 0.1 mol/L of hydrochloric acid-mixed solution, and adjust the pH to 3.0. The mixed solution was placed in a water bath thermostatic oscillator at a reaction temperature of 25 °C and a rotating speed of 160 r/min for 120 min, and the sample was taken, filtered by 0.45 μm water filter membrane, and the concentration of the filtrate was determined by ICP-OES. The filter slag was placed in a 200 mL conical bottle, and 100 mL of sodium hydroxide solution with a concentration of 0.1 mol/L was dropped into the water bath constant temperature oscillator with a reaction temperature of 25 °C and a rotating speed of 160 r/min. After the desorbing reaction, the filter slag was filtered and washed until the pH of the cleaning solution was neutral, and then the regeneration was completed by drying treatment. The experiment was repeated with recycled material.

(5) Kinetics and isotherm fitting

In this paper, quasi-first-order and quasi-second-order kinetic models were used to fit the adsorption process of As (V) on magnetic micro-nano composites, and the adsorption kinetics of As (V) on magnetic micro-nano composites were studied.

Quasi-first-order kinetic model equation:

$$Q_t = Q_e \left[1 - \exp(-K_1 t)\right] \tag{1}$$

Quasi-second-order kinetic model equation:

$$Q_t = Q_e \left[1 - \frac{1}{1 + Q_e K_2 t}\right] \tag{2}$$

where, Q_e is the adsorption amount of magnetic micro-nano composite at equilibrium adsorption of As (V), mg·g^{-1}; Q_t is the adsorption capacity of magnetic micro-nano composite for As (V) at time t, mg·g^{-1}; K_1 is the quasi-first-order kinetic parameter, min^{-1}; and K_2 is the quasi-second-order kinetic parameters, g·(mg·min)$^{-1}$.

In this paper, Langmuir and Freundlich isothermal models were used to fit the experimental data, and the relationship between the adsorption capacity of magnetic micro-nano composites and the equilibrium concentration of As (V) was studied, and the maximum adsorption capacity of magnetic micro-nano composites was further predicted.

Langmuir model equation:

$$Q_e = \left(\frac{Q_m K_L C_e}{1 + K_L C_e}\right) \tag{3}$$

Freundlich model equation:

$$Q_e = K_F C_e^{\frac{1}{n}} \tag{4}$$

where, Q_e is the adsorption amount of magnetic micro-nano composite at equilibrium adsorption of As (V), mg/g; Q_m is the maximum adsorption capacity of magnetic micro-nano composite for As (V), mg/g; C_e is the concentration at equilibrium, mg/L; K_L is the Langmuir equilibrium adsorption constant, L/mg; K_F is the Freundlich adsorption constant; and n is the Adsorption strength.

3. Results

3.1. Comparison of NdFeB Secondary Waste and Magnetic Micro-Nano Composite Materials

(1) As (V) Removal Rate of Micro-nano Composite Materials and NdFeB secondary waste

From the analysis of Figure 2, it can be seen that the As (V) removal rate of NdFeB secondary waste in the reaction time of 120 min is only 56.43%, the As (V) removal rate of magnetic micro-nano composite materials is greatly increased to 96.43%.
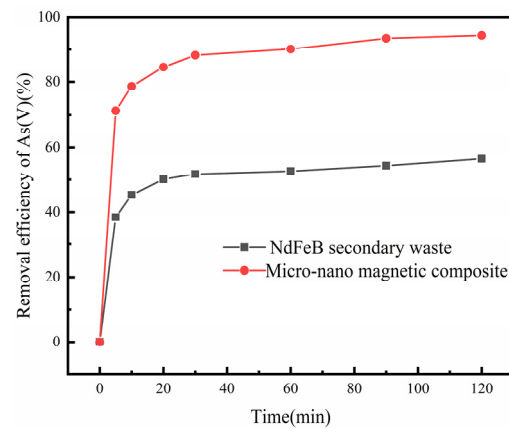
Figure 2. As (V) Removal Rate of Micro-nano Composite Materials and NdFeB secondary waste.

(2) Crystal structure before and after mechanochemical activation

The XRD pattern of the material before and after mechanochemical activation was obtained by the X-ray diffractometer in Figure 3.
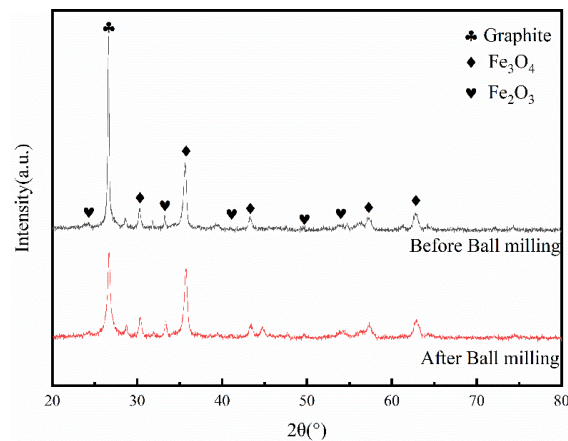

Figure 3. XRD patterns of the raw powder and magnetic micro-nano composite materials.

According to the analysis in Figure 3, the main components of NdFeB secondary waste are graphite, Fe_3O_4, and Fe_2O_3. After mechanical mechanochemical activation, the diffraction peak strength of NdFeB secondary waste is significantly weakened, which indicates that the crystal structure of the material is damaged under the mechanical mechanochemical action, and the material is transformed from crystal structure to amorphous state, and its amorphous degree is deepened [28]. The presence of this amorphous phase can increase the strength of the interaction between the adsorbent and the adsorbent, thereby improving the adsorption capacity of the material for As (V) [29].

(3) The changes in material morphology before and after mechanochemical activation:

The SEM images before and after mechanochemical activation and the mapping images of C, O, and Fe elements on the surface of the material before and after mechanochemical activation were obtained by field emission scanning electron microscopy (SEM)-energy spectrometer (EDS).

From the analysis of Figure 4, it can be seen that the raw materials without mechanical force chemical activation before the particle size is large and the powder particles are seriously agglomerated, in the mechanical force chemical activation of the material, the micro-morphology of the material has been significantly changed, and the material particles in the mechanical force chemical action of the particle size are significantly reduced. In addition, the mechanical chemical activation effectively eliminates the agglomeration between the material particles and makes the material particles more dispersed.
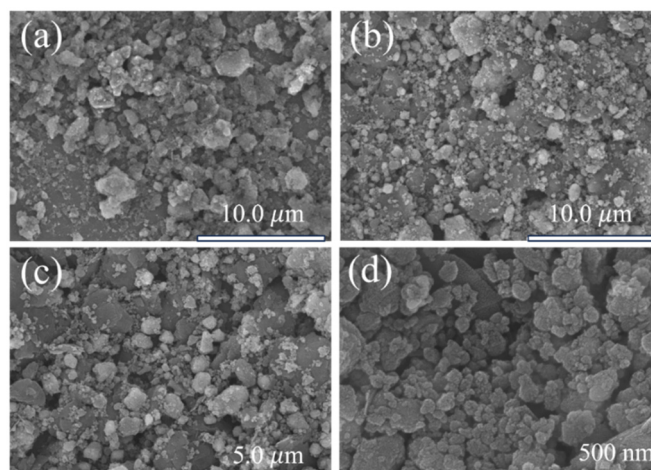
Figure 4. SEM image of the raw powder (**a**) and magnetic micro-nano composite materials (**b–d**).

It can be seen from the analysis of Figure 5 that Fe element agglomeration is more serious on the surface of NdFeB secondary waste material, and Fe element distribution is more uniform after mechanical mechanochemical activation, which indicates that the exposure of iron oxide can be increased under mechanical mechanochemical action, so that iron oxide can be more evenly distributed on the surface of the material, which is favorable for the complex reaction between the material and arsenate ion in the solution.
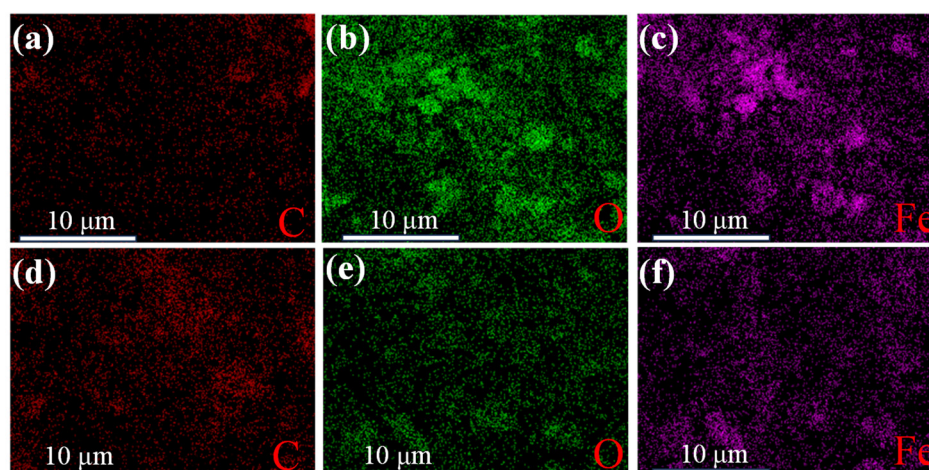

Figure 5. Mapping diagram: (**a–c**) NdFeB secondary waste, (**d–f**) magnetic micro-nano composite materials.

(4) The changes in chemical bonds and functional groups of materials before and after mechanochemical activation

It can be seen from the analysis of Figure 6 that the raw materials mainly have the following characteristics: Fe-O stretching vibration characteristics peak at 466 cm^{-1} [29], Fe-OH bending vibration characteristics peak at 590 cm^{-1}, C-O stretching vibration characteristic peak at 1090 cm^{-1}. H-O-H water molecule bending vibration characteristics peak located at 1635 cm^{-1}, and O-H stretching vibration characteristic peak located at 3420 cm^{-1} [30]. After mechanochemical activation, these functional groups and chemical bonds changed to different degrees, and the strength of Fe-O stretching vibration characteristic peak, Fe-OH bending vibration characteristic peak, and C-O stretching vibration characteristic peak increased significantly and produced a small amount of deviation. Among them, the increase in bending vibration characteristic peak-peak strength of Fe-OH after mechanical mechanochemical activation means an increase in Fe-OH content, and Fe-OH will react with arsenate ions in solution to produce complexes to remove arsenic

pollution, which is also one of the main reasons for the significant increase in the As (V) removal rate of materials after mechanical mechanochemical activation.
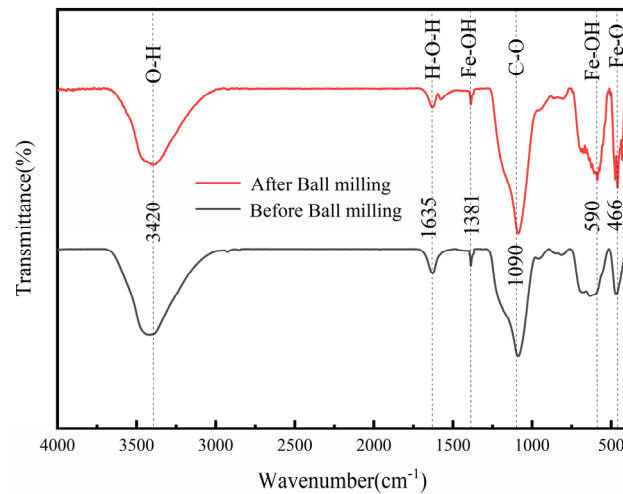

Figure 6. FT-IR patterns of the raw powder and magnetic micro-nano composite materials.

3.2. As (V) Removal by Magnetic Micro-Nano Composite Materials

(1) Test on the effect of initial pH of solution on the removal rate of As (V):

The initial pH value of the solution can affect the whole reaction process by changing the existence, form, and chemical properties of arsenic pentavalent in the solution and the surface charge of the adsorbed material [31]. When the initial pH of the solution is less than 2.0, As (V) exists in the solution mainly in the form of neutral H_3AsO_4 molecules; when the initial pH of the solution is between 2.0 and 7.0, As (V) exists in the solution mainly in the form of negatively charged H_2AsO_4 ions; and when the initial pH of the solution is between 7.0 and 11.0, As (V) exists in the solution mainly in the form of negatively charged $HAsO_4^{2-}$ ions [32]. Figure 7a shows the effect of magnetic micro-nano composites on the As (V) removal rate and Zeta potential value at the initial pH values of different solutions (1.0, 3.0, 5.0, 7.0, 9.0, and 11.0). As can be seen from the figure, the removal rate of As (V) and the Zeta potential value of magnetic micro-nano composites are significantly affected by the initial pH value of the solution. The effect of initial pH value of the solution on the removal of As (V) from magnetic micro-nano composites is first increased and then decreased, and the Zeta potential value of the material significantly decreased with the increase in the initial pH value of the solution. When the initial pH value of the solution was 1.0, the As (V) removal rate of the magnetic micro-nano composite was only 63.00%, and with the increase in the initial pH value of the solution, the As (V) removal rate of the magnetic micro-nano composite also increased, reaching the maximum of 94.33% when the pH value was 3.0, and then with the increase in the initial pH value of the solution, the removal rate of As (V) from the magnetic micro-nano composite decreases gradually and decreases to 45.29% when the initial pH value of the solution is 11.0. The analysis shows that As (V) exists in the form of neutral H_3AsO_4 molecules in the solution when the initial pH value is 1.0, and the removal of As (V) by magnetic micro-nano composite is less affected by the electrostatic effect. On the other hand, the partial dissolution of magnetic micro-nano composites under the condition of strong acid results in a reduction of effective adsorption sites on the surface of the material. Therefore, the As (V) removal effect of the material is significantly reduced. Subsequently, As the initial pH value of the solution increased, the degree of deprotonation on the surface of the magnetic micro-nano composite became deeper, resulting in an increase in negative charge on the surface of the material and a decrease in the Zeta potential value of the material. As a result, the electrostatic attraction effect between the negatively charged arsenate ion and the adsorption site on the surface of the magnetic micro-nano composite was weakened, and the As (V) removal rate of the material was reduced. In addition, it can be seen from the figure that the zero-point

potential pH$_{zpc}$ of the magnetic micro-nano composite material is 9.1, that is, when the pH is 9.1, the amount of negative and positive charges on the surface of the material is the same, and the net charge on the surface of the material is zero. When the pH value of the solution is greater than the zero potential pH$_{zpc}$, the surface of the material is negatively charged, and when the pH value of the solution is less than the zero potential pH$_{zpc}$, the surface of the material is positively charged. When the pH is greater than 9.1, the net charge on the surface of the material is negative, which repels the arsenate ions, which is also the reason why the removal rate of the material decreases significantly when the pH is 11.0. Therefore, pH 3.0 was determined to be the best initial pH value of the solution for the test.
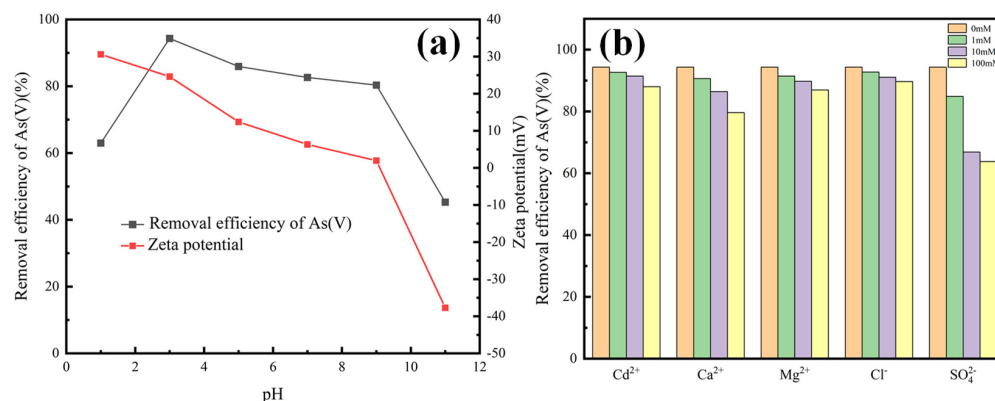

Figure 7. As (V) removal by magnetic micro-nano composite materials: (**a**) effect of solution pH, (**b**) effect of competition ions.

(2) Test on the influence of coexisting ions on the removal rate of As (V):

In the actual mine wastewater containing As (V), it is inevitable that many coexisting ions compete with arsenate ions for the adsorption sites of adsorption materials. Therefore, in order to simulate the real wastewater environment, the common cations (Cd^{2+}, Ca^{2+}, mg^{2+}) and anions (Cl^-, SO_4^{2-}) in the wastewater are selected as coexisting ions. Three concentration gradients of 1, 10, and 100 mM were selected to investigate the effects of these coexisting ions on the removal of As (V) from magnetic micro-nano composites. Figure 7b shows the effect of coexisting ions on the removal rate of As (V) in magnetic micro-nano composites. It can be seen from the figure that the order of influence of cations on the material removal rate is as follows: $Ca^{2+} > mg^{2+} > Cd^{2+}$. The overall effect is small, among which the highest effect is 79.61% removal of As(V) by micro- and nano-magnetic composites at Ca^{2+} concentration of 100 mM and the lowest effect is 88.01% removal of As(V) by micro- and nano-magnetic composites at Cd^{2+} concentration of 100 mM. It shows that the affinity of the magnetic micro-nano composite to arsenate ions is much higher than that of the above three cations. The Cl^- in the anion has little effect on the removal of As (V) by the magnetic micro-nano composite. When the concentration of Cl^- is 100 mM, the removal rate of As (V) by the magnetic micro-nano composite is still 89.65%, which only decreases by 3.79%. This is because the negative valence of Cl^- does not participate in or a small amount of competition with arsenate ions for effective adsorption sites on the surface of magnetic micro-nano composite materials. SO_4^{2-} has the greatest influence on the material removal rate. When the concentration is 100 mM, the material's removal rate of As (V) is 63.76%, which is because the negative bivalent SO_4^{2-} ion has an electrostatic effect with the negatively charged arsenate ion and forms a competitive adsorption relationship, which reduces the material's removal rate of As (V). The above experimental studies show that the magnetic micro-nano composite still has a good removal effect on As (V) in the presence of coexisting ions in the solution, so the magnetic micro-nano composite is suitable for treating complex arsenic polluted wastewater in practical application.

3.3. Regeneration of Magnetic Micro-Nano Composite Materials

To evaluate the application potential of magnetic micro-nano composites, the repetitive regeneration performance was investigated. The hydroxide in NaOH solution can undergo coordination exchange with the arsenate ion on the surface of the material after adsorption of As (V), thus achieving the purpose of regenerating the material [33]. Therefore, in this experiment, 0.1 mol/L NaOH solution was used desorb As (V) adsorbed by magnetic micro-nano composite material. Figure 8 shows the removal efficiency of the magnetic micro-nano composite material for As (V) after repeated regeneration five times, as shown in the figure. After five adsorption–desorption cycles, the magnetic micro-nano composite still has a good removal effect on As (V). With the increase in the number of cycles, the removal rate of As (V) of the magnetic micro-nano composite decreases from 94.33% to 73.56%, but it is still much higher than that of the raw materials without mechanical and chemical activation. It is concluded that the As (V) removal rate of the regenerated magnetic micro-nano composite decreases due to the inevitable loss of the material during the adsorption–desorption cycle and the fact that the effective adsorption site on the surface of the material is continuously occupied by the arsenate ion and the functional group is continuously weakened. In addition, the surface charge of the material changes, and the electrostatic effect on arsenate ions is weakened. The As (V) removal ability of the magnetic micro-nano composite was reduced after repeated regeneration. The excellent repeatability of magnetic micro-nano composite material reduces its use cost, so the magnetic micro-nano composite material has great application potential and economic benefits in the treatment of As (V)-containing wastewater in actual mines.
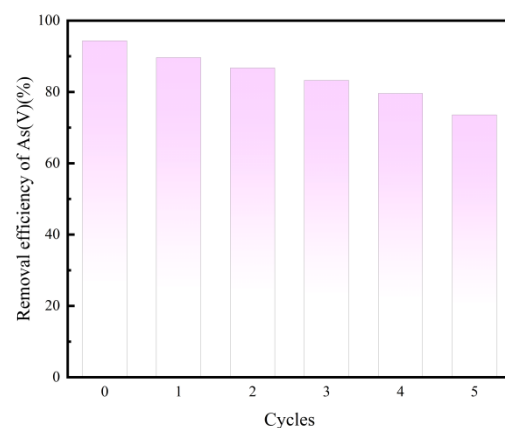

Figure 8. The effect of cycle regeneration frequency on As (V) removal rate.

3.4. Kinetics for As (V) Uptake

Adsorption kinetics is a curve used to describe the adsorption rate of adsorbents [13]. In this study, the quasi-first-order kinetic model and quasi-second-order kinetic model were used to fit the adsorption process of magnetic micro-nano composite As (V), and the adsorption kinetics of As (V) on the magnetic micro-nano composite were studied with the intention of studying the adsorption mechanism. Figure 9a shows the adsorption kinetics of As (V) on magnetic micro-nano composites and the fitting diagram of its quasi-first-order/second-order model. Table 2 shows the fitting parameters of the quasi-first-order kinetic model and quasi-second-order kinetic model. As can be seen from the Figure 9a, the quasi-second-order kinetic model has the best fitting effect on the adsorption of As (V) by magnetic micro-nano composite materials, where the correlation coefficient R^2 is as high as 0.9977 and the theoretical adsorption capacity is 9.459 mg/g, which is close to the actual adsorption capacity (9.471 mg/g). Therefore, it can be seen that the adsorption of magnetic micro-nano composite materials for As (V) is more inclined to chemical adsorption, and the adsorption process mainly depends on the complex reaction between the functional groups on the magnetic micro-nano composite materials and arsenate ions.
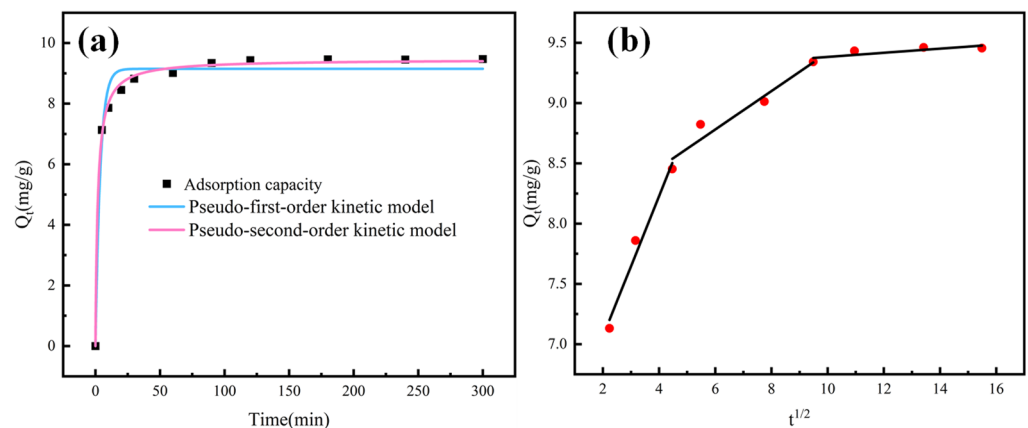
Figure 9. (**a**) Kinetics adsorption of As (V) on magnetic micro-nano composite materials and pseudo-first/second-order fitting. (**b**) Intraparticle diffusion model of As (V) adsorption on magnetic micro-nano composite materials.

Table 2. Fitting parameters of adsorption kinetics of As (V) on magnetic micro-nano composite materials.

PFO Kinetic Model			PSO Kinetic Model		
Q_e (mg.g^{-1})	K_1 (min^{-1})	R^2	Q_e (mg/g)	K_2 (g.mg^{-1}.min^{-1})	R^2
9.148	0.266	0.9772	9.459	0.0579	0.9977

Considering the porous properties of magnetic micro-nano composites, the internal diffusion behavior in the adsorption of As (V) cannot be ignored. In order to determine the internal diffusion behavior of As (V) during the adsorption of magnetic micro-nano composites, the in-particle diffusion model was fitted to the adsorption kinetic data of As (V) on magnetic micro-nano composites. Figure 9b shows the in-particle diffusion model of magnetic micro-nano composites adsorbed with As (V). As can be seen from the figure, the fitting result of the in-particle diffusion model consists of three linear parts, indicating that the adsorption of As (V) by magnetic micro-nano composite materials can be divided into three stages. The first stage is the rapid adsorption stage, in which many adsorption sites are exposed on the surface of the magnetic micro-nano composite material, and arsenate ions rapidly diffuse from the solution to the surface of the magnetic micro-nano composite material to occupy the adsorption site. The second stage is the intra-particle diffusion stage, in which most of the effective adsorption sites on the surface of the magnetic micro-nano composite have been occupied, and arsenate ions diffuse to the inner surface of the material through the pore size, occupying the internal adsorption sites of the material, and the adsorption rate gradually slows down. The third stage is the adsorption equilibrium stage, in which the arsenate ion gradually occupies the adsorption site in the pores of the magnetic micro-nano composite material, and the adsorption rate approaches zero, reaching the adsorption equilibrium state. In addition, the line fitted in the fitting diagram does not have an origin, indicating that the adsorption rate of the magnetic micro-nano composites for As (V) is limited by intra-particle diffusion and is also affected by other factors such as film diffusion and surface adsorption [34].

3.5. As (V) Uptake Isotherms

The adsorption isotherm is a curve used to describe the concentration relationship between the liquid and solid phases in the reaction equilibrium at constant temperature [35]. To further understand the adsorption mechanism, study the relationship between the adsorption capacity of magnetic micro-nano composite materials and the equilibrium concentration of As (V) and further predict the maximum adsorption capacity of magnetic micro-nano composite materials. In this paper, Langmuir and Freundlich isothermal

models were used to fit the test data. The fitting results are shown in Figure 10, and the fitting parameters are shown in Table 3.
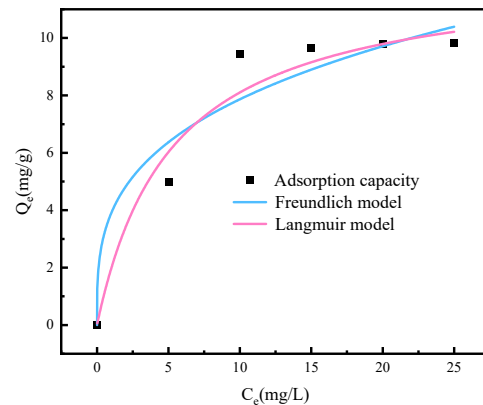

Figure 10. The adsorption isotherm of As (V) on magnetic micro-nano composite materials and Langmuir and Freundlich model fitting.

Table 3. Adsorption isotherm fitting parameters of As (V) on magnetic micro-nano composite materials.

Langmuir Model			Freundlich Model		
Q_m (mg.g^{-1})	K_L (L.mg^{-1})	R^2	K_F	n	R^2
10.477	0.189	0.853	25.62	0.25	0.793

As can be seen from Figure 10, the adsorption capacity of magnetic micro-nano composites for As (V) increases first and then tends to balance with the increase in the equilibrium concentration of As (V). The Langmuir isothermal model has the best fitting effect on the adsorption of magnetic micro-nano composites for As (V), for which the correlation coefficient R^2 is 0.853. The theoretical maximum adsorption capacity is 10.477 mg/g, which indicates that the adsorption of As (V) on the surface of magnetic micro-nano composite materials is more inclined to single-molecular layer adsorption, and As (V) is uniformly adsorbed on the surface of magnetic micro-nano composite materials.

3.6. Surface Analysis of As (V)-Adsorbed Magnetic Micro-Nano Composite Materials

(1) Zeta potential analysis

Figure 11a shows the variation of the Zeta potential with the pH value of the solution before and after adsorption of As (V) by magnetic micro-nano composite. It can be seen from the figure that the Zeta potential of magnetic micro-nano composites before and after adsorption of As (V) decreases with the increase in pH value, the Zeta potential value of magnetic micro-nano composites after adsorption of As (V) decreases significantly, and the zero-point potential pHzpc of magnetic micro-nano composites before adsorption of As (V) is 9.1. After adsorption of As (V), the zero-point potential of the magnetic micro-nano composite decreases to 5.6. Studies have shown that the specific adsorption of anions, namely chemisorption, can make the anions form an inner layer complex with the adsorption material, and the surface of the adsorption material has more negative charges, thus reducing the Zeta potential of the material and moving the zero point potential to the low pH region [36]. In contrast, if the anion interacts electrostatically with the adsorbed material only through non-specific adsorption, the Zeta potential of the material does not change. Therefore, according to the Zeta potential characterization test results after adsorption of As (V), it can be inferred that there is not only a simple electrostatic attraction between As (V) and magnetic micro-nano composite materials but also chemical adsorption. Covalent bonds are formed between the arsenate ion and the material, and a complex is generated, resulting in a decline in Zeta potential of the material after adsorption of As (V).
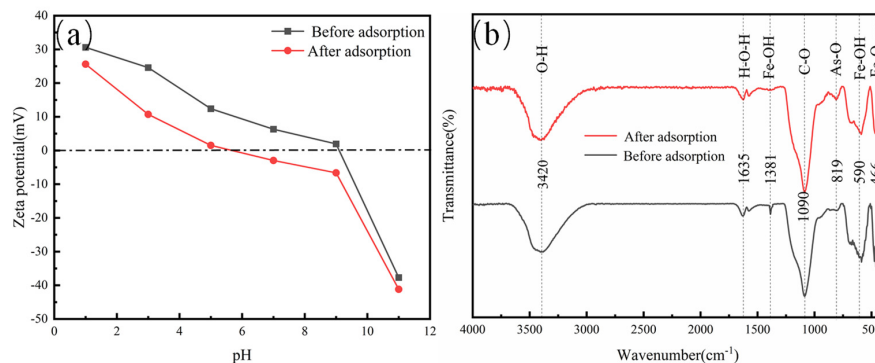
Figure 11. (**a**) Zeta potential of magnetic micro-nano composite materials before and after As (V) uptake and (**b**) FTIR spectra of magnetic micro-nano composite materials before and after As (V) uptake.

(2) FT-IR spectrogram analysis

Figure 11b shows the FT-IR spectra of magnetic micro-nano composites before and after adsorption of As (V). It can be seen from the figure that before adsorption of As (V), the magnetic micro-nano composite material has the following characteristic peaks: Fe-O stretching vibration peak at 466 cm^{-1}, Fe-OH bending and stretching vibration peak at 590 cm^{-1} and 1381 cm^{-1}. C-O stretching vibration characteristics peak located at 1090 cm^{-1}, H-O-H water molecule bending vibration characteristics peak located at 1635 cm^{-1}, and O-H stretching vibration characteristics peak located at 3420 cm^{-1}. The FT-IR spectra of the material after adsorption As (V) showed that the characteristic peaks of Fe-O stretching vibration, Fe-OH bending vibration, C-O stretching vibration, H-O-H bending vibration and H-O stretching vibration did not significantly shift or stretch. These results indicate that these functional groups do not play a role in or participate in the reaction of magnetic micro-nano composite materials with As (V). The strength of the Fe-OH stretching vibration characteristic peak at 1381 cm^{-1} decreased significantly after adsorption of As (V) by magnetic micro-nano composites, indicating that hydroxyl groups were involved in the adsorption process. The adsorption of As (V) by magnetic micro-nano composites followed the inner sphere coordination mechanism, which was consistent with the surface charge analysis results. In addition, FT-IR spectra of the material after adsorption of As (V) also showed a new characteristic peak at 819 cm^{-1}, which is the characteristic peak of the stretching vibration of AS-O [37] according to literature review, indicating that arsenic is successfully adsorbed on the surface of the magnetic micro-nano composite material and that covalent bonds are formed between arsenate ions and the material. The analysis results are consistent with the fitting results of the adsorption kinetics model.

(3) XPS spectral analysis

Figure 12 shows the XPS spectrum of magnetic micro-nano composite materials before and after adsorption of As (V). It can be seen from Figure 12a that the position and intensity of the Fe2p peak before and after adsorption of As (V) have little change. The binding energy of Fe2p$_{1/2}$ is about 724.0 eV, the binding energy of Fe2p$_{3/2}$ is about 710.8 eV, and the shock excitation effect is about 719.0 eV. This indicates that before and after adsorption of As (V), iron mainly exists in the form of trivalent iron oxide [38]. Figure 12b is the As3d fine spectrum. As shown in the figure, the characteristic peak of As (V) appears at the binding energy position of 45.6 eV [39], which once again proves that As (V) is successfully adsorbed on the magnetic micro-nano composite material, and no characteristic peak of other valence arsenics appears. The results indicated that As (V) did not undergo a REDOX reaction during the adsorption process of the magnetic micro-nano composite and As (V) and arsenic was adsorbed on the magnetic micro-nano composite in the pentavalent form. Figure 12c is a fine spectrum of C1s, from which it can be seen that the characteristic peak intensity and position of carbon-containing functional groups did not change significantly before and after the magnetic micro-nano composite adsorbed As (V), indicating that element C did not play a role or participate in the reaction between the magnetic micro-

nano composite and As (V) [40]. Figure 12d is the fine spectrum of O1s. As shown in the figure, there are mainly three different oxygen-containing functional groups of element O, namely H_2O, Fe-OH, and Fe-O. The relative content of Fe-OH decreased from 38.33 to 30.42% after the reaction of magnetic micro-nano composites with As (V), indicating that Fe-OH on the surface of magnetic micro-nano composites plays a key role in the adsorption of As (V). This analysis result is consistent with that of FT-IR analysis.
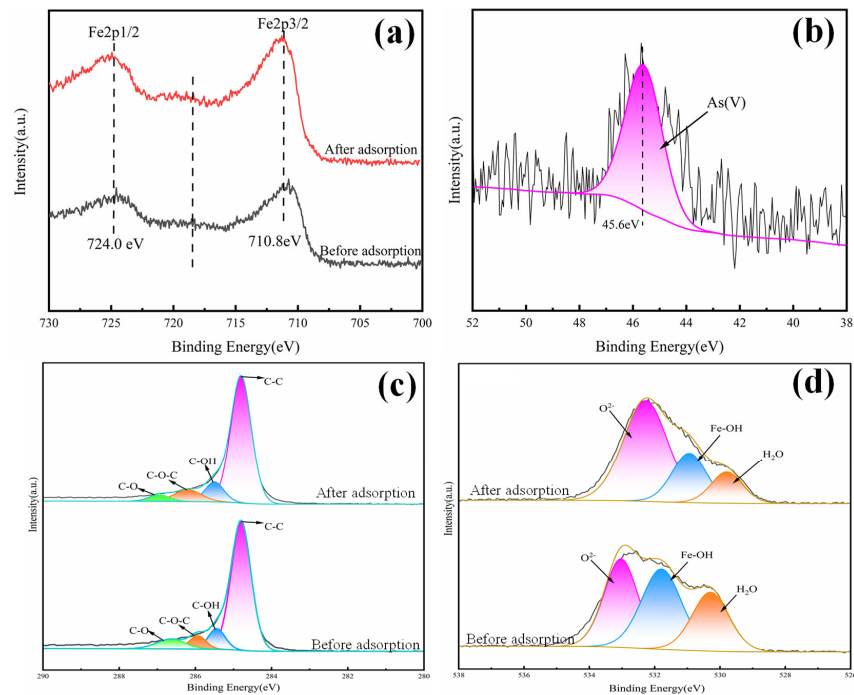

Figure 12. XPS spectra of magnetic micro-nano composite materials before and after As (V) adsorption: (**a**) Fe2p, (**b**) As3d, (**c**) C1s, and (**d**) O1s.

3.7. As (V) Removal Mechanisms

From the above analysis, it can be seen that the removal mechanism of As (V) by magnetic micro-nano composites is that arsenate ions in solution rapidly diffuse to the surface of magnetic micro-nano composites through electrostatic attraction, and then arsenate ions and metal hydroxyl groups (Fe-OH) on the surface of magnetic micro-nano composites undergo coordination exchange reaction to form an inner spherical complex. Arsenate ion is fixed in the pore of the material, and the removal mechanism is shown in Figure 13.
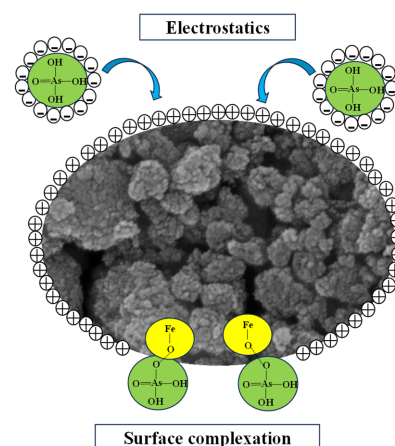

Figure 13. Governing mechanisms of As (V) removal by magnetic micro-nano composite materials.

4. Conclusions

In this study, the NdFeB secondary waste was activated by the mechanical mechanochemical method, and the micro-nano magnetic composite material was successfully prepared for the treatment of As (V)-containing wastewater in mines. The As (V) removal performance and mechanism of micro-nano magnetic composite material were studied. The main components of the NdFeB secondary waste are Fe_2O_3, Fe_3O_4, and C. After mechanochemical activation, the material particles become more dispersed, the particle size decreases significantly, and the specific surface area increases significantly. At the same time, the diffraction peak strength of the material decreases significantly, indicating the transformation from crystal structure to amorphous structure, and the degree of amorphism increases. In addition, after mechanochemical activation, the peak-to-peak strength of Fe-OH flexural vibration of the magnetic micro-nano composite increases, indicating that the Fe-OH content increases. The experimental results of removing the wastewater containing As (V) show that the treatment results are best when the initial solution pH is 3. Combined with Zeta potential analysis, it is concluded that the material removal process of As (V) is affected by electrostatic adsorption. In addition, the material is less affected by coexisting ions and still maintains a high removal rate of As (V) in the presence of high concentrations of coexisting ions, which has great application potential. The kinetic and isotherm fitting results show that the adsorption process of As (V) is more consistent with the quasi-second-order kinetic model and Langmuir isothermal model, indicating that the removal of As (V) by the material is more biased towards chemisorption and single molecular layer adsorption, and the theoretical maximum adsorption capacity is 10.477 mg/g. Zeta, FT-IT, and XPS characterization tests confirm that the removal of As (V) depends on the coordination exchange reaction between the material and As (V) to form the inner sphere complex. After five repeated regeneration tests, the material still maintains a high removal rate of As (V), which proves that the micro-nano magnetic composite material generated by NdFeB secondary waste under the action of high-energy ball milling is used to remove As (V) in water, which has low cost, green environmental protection, and high economic benefits.

Author Contributions: Conceptualization, X.F.; methodology, X.F.; validation, Y.R.; formal analysis, X.F. and Y.R.; investigation, X.F. and Y.R.; resources, X.F.; data curation, X.F. and Y.R.; writing—original draft, Y.R.; writing—review and editing, X.F.; visualization, Y.R.; supervision, X.F. and Y.R.; project administration, X.F. and Y.R.; funding acquisition, X.F. All authors have read and agreed to the published version of the manuscript.

Data Availability Statement: The data are not publicly available due to agency management. Data was obtained from China University of Mining and Technology, and are available from the authors with the permission of China University of Mining and Technology.

Conflicts of Interest: Author Xiujuan Feng was employed by the company Ji'an Xintai Technology Co., Ltd. The remaining authors declare that the research was conducted in the absence of any commercial or financial relationships that could be construed as a potential conflict of interest.

References

1. Peiró, L.T.; Méndez, G.V.; Ayres, R.U. Material flow analysis of scarce metals: Sources, functions, end-uses and aspects for future supply. *Environ. Sci. Technol.* **2013**, *47*, 2939–2947. [CrossRef] [PubMed]
2. Sagawa, M.; Fujimura, S.; Yamamoto, H.; Matsuura, Y.; Hiraga, K. Permanent magnet materials based on the rare earth-iron-boron tetragonal compounds. *IEEE Trans. Magn.* **1984**, *20*, 1584–1589. [CrossRef]
3. Schulze, R.; Buchert, M. Estimates of global REE recycling potentials from NdFeB magnet material. *Resour. Conserv. Recycl.* **2016**, *113*, 12–27. [CrossRef]
4. Shirayama, S.; Okabe, T.H. Selective Extraction and Recovery of Nd and Dy from Nd-Fe-B Magnet Scrap by Utilizing Molten $MgCl_2$. *Met. Mater. Trans. B* **2018**, *49*, 1067–1077. [CrossRef]
5. Venkatesan, P.; Hoogerstraete, T.V.; Hennebel, T.; Binnemans, K.; Sietsma, J.; Yang, Y. Selective electrochemical extraction of REEs from NdFeB magnet waste at room temperature. *Green Chem.* **2018**, *20*, 1065–1073. [CrossRef]

6. Kumari, A.; Sinha, M.K.; Pramanik, S.; Sahu, S.K. Recovery of rare earths from spent NdFeB magnets of wind turbine: Leaching and kinetic aspects. *Waste Manag.* **2018**, *75*, 486–498. [CrossRef] [PubMed]

7. Liu, B.; Zhu, N.; Li, Y.; Wu, P.; Dang, Z.; Ke, Y. Efficient recovery of rare earth elements from discarded NdFeB magnets. *Process Saf. Environ. Prot.* **2019**, *124*, 317–325. [CrossRef]

8. Özkaraaslan, H.; Çetintaş, S.; Bingöl, D. A novel composite derived from carbonized hawthorn waste pulp/marble waste powder by ball milling: Preparation, characterization, and usability as bifunctional adsorbent. *Biomass Convers. Biorefinery* **2021**, *13*, 3765–3784. [CrossRef]

9. Do, J.-L.; Friščić, T. Mechanochemistry: A Force of Synthesis. *ACS Cent. Sci.* **2016**, *3*, 13–19. [CrossRef] [PubMed]

10. Chen, Z.; Lu, S.; Mao, Q.; Buekens, A.; Chang, W.; Wang, X.; Yan, J. Suppressing Heavy Metal Leaching through Ball Milling of Fly Ash. *Energies* **2016**, *9*, 524. [CrossRef]

11. Wang, M.-M.; Zhang, C.-C.; Zhang, F.-S. An environmental benign process for cobalt and lithium recovery from spent lithium-ion batteries by mechanochemical approach. *Waste Manag.* **2016**, *51*, 239–244. [CrossRef] [PubMed]

12. Zou, H.; Zhao, J.; He, F.; Zhong, Z.; Huang, J.; Zheng, Y.; Zhang, Y.; Yang, Y.; Yu, F.; Bashir, M.A.; et al. Ball milling biochar iron oxide composites for the removal of chromium (Cr(VI)) from water: Performance and mechanisms. *J. Hazard. Mater.* **2021**, *413*, 125252. [CrossRef] [PubMed]

13. Li, F.; Wan, Y.; Chen, J.; Hu, X.; Tsang, D.C.W.; Wang, H.; Gao, B. Novel ball-milled biochar-vermiculite nanocomposites effectively adsorb aqueous As(V). *Chemosphere* **2020**, *260*, 127566. [CrossRef] [PubMed]

14. Shiyang, X.; Ziling, S.; Xiaoliang, Z.; Jiyang, L. Review of the recent advances in the prevention, treatment, and resource recovery of acid mine wastewater discharged in coal mines. *J. Water Process Eng.* **2023**, *52*, 103555. [CrossRef]

15. Ran, H.; Guo, Z.; Yi, L.; Xiao, X.; Zhang, L.; Hu, Z.; Li, C.; Zhang, Y. Pollution characteristics and source identification of soil metal(loid)s at an abandoned arsenic-containing mine, China. *J. Hazard. Mater.* **2021**, *413*, 125382. [CrossRef] [PubMed]

16. Glenna, T.; Craig, S.; Peter, E.H. Arsenic contamination and rare earth element composition of acid mine drainage impacted soils from South Africa. *Miner. Eng.* **2023**, *203*, 108288. [CrossRef]

17. Wang, S.; Zheng, K.; Li, H.; Feng, X.; Wang, L.; Liu, Q. Arsenopyrite weathering in acidic water: Humic acid affection and arsenic transformation. *Water Res.* **2021**, *194*, 116917. [CrossRef] [PubMed]

18. Nordstrom, D.K.; Alpers, C.N. Negative pH, efflorescent mineralogy, and consequences for environmental restoration at the Iron Mountain Superfund site, California. *Proc. Natl. Acad. Sci. USA* **1999**, *96*, 3455–3462. [CrossRef] [PubMed]

19. Burton, E.D.; Karimian, N.; Johnston, S.G.; Schoepfer, V.A.; Choppala, G.; Lamb, D. Arsenic-Imposed Effects on Schwertmannite and Jarosite Formation in Acid Mine Drainage and Coupled Impacts on Arsenic Mobility. *ACS Earth Space Chem.* **2021**, *5*, 1418–1435. [CrossRef]

20. Luo, C.; Routh, J.; Dario, M.; Sarkar, S.; Wei, L.; Luo, D.; Liu, Y. Distribution and mobilization of heavy metals at an acid mine drainage affected region in South China, a post-remediation study. *Sci. Total Environ.* **2020**, *724*, 138122. [CrossRef] [PubMed]

21. Zhu, J.; Zhang, P.; Yuan, S.; Tong, M. Arsenic oxidation and immobilization in acid mine drainage in karst areas. *Sci. Total Environ.* **2020**, *727*, 138629. [CrossRef] [PubMed]

22. Mohammad, T.A.; Sebastián, S.; Julio, S.; Bernabé, L.R. Arsenic oxidation and its subsequent removal from water: An overview. *Sep. Purif. Technol.* **2022**, *309*, 123055. [CrossRef]

23. Jadhav, S.V.; Bringas, E.; Yadav, G.D.; Rathod, V.K.; Ortiz, I.; Marathe, K.V. Arsenic and fluoride contaminated groundwaters: A review of current technologies for contaminants removal. *J. Environ. Manag.* **2015**, *162*, 306–325. [CrossRef] [PubMed]

24. Verma, S.; Kuila, A. Bioremediation of heavy metals by microbial process. *Environ. Technol. Innov.* **2019**, *14*, 100369. [CrossRef]

25. Fischer, A.; Lee, M.-K.; Ojeda, A.S.; Rogers, S.R. GIS interpolation is key in assessing spatial and temporal bioremediation of groundwater arsenic contamination. *J. Environ. Manag.* **2020**, *280*, 111683. [CrossRef] [PubMed]

26. Abidli, A.; Huang, Y.; Ben Rejeb, Z.; Zaoui, A.; Park, C.B. Sustainable and efficient technologies for removal and recovery of toxic and valuable metals from wastewater: Recent progress, challenges, and future perspectives. *Chemosphere* **2021**, *292*, 133102. [CrossRef] [PubMed]

27. Fan, L.; Zhao, F.; Liu, J.; Frost, R.L. The As behavior of natural arsenical-containing colloidal ferric oxyhydroxide reacted with sulfate reducing bacteria. *Chem. Eng. J.* **2017**, *332*, 183–191. [CrossRef]

28. Lei, Z.; Cagnetta, G.; Li, X.; Qu, J.; Li, Z.; Zhang, Q.; Huang, J. Enhanced adsorption of potassium nitrate with potassium cation on H_3PO_4 modified kaolinite and nitrate anion into Mg-Al layered double hydroxide. *Appl. Clay Sci.* **2018**, *154*, 10–16. [CrossRef]

29. Wang, P.; Hu, J.; Wang, Y.; Liu, T. Enhanced elimination of V5+ in wastewater using zero-valent iron activated by ball milling: The overlooked crucial roles of energy input and sodium chloride. *J. Hazard. Mater.* **2022**, *435*, 129050. [CrossRef] [PubMed]

30. Fu, X.; Wang, X.; Leung, D.Y.C.; Gu, Q.; Chen, S.; Huang, H. Photocatalytic reforming of C3-polyols for H_2 production. *Appl. Catal. B Environ. Energy* **2011**, *106*, 681–688. [CrossRef]

31. Wang, H.; Wang, S.; Zhao, M.; Li, Y.; Kong, F. Removal of arsenic from aqueous solution using microflower-like δ-Bi_2O_3 as adsorbent: Adsorption characteristics and mechanisms. *J. Dispers. Sci. Technol.* **2019**, *41*, 2026–2036. [CrossRef]

32. Vieira, B.R.C.; Pintor, A.M.A.; Boaventura, R.A.R.; Botelho, C.M.S.; Santos, S.C.R. Arsenic removal from water using iron-coated seaweeds. *J. Environ. Manag.* **2017**, *192*, 224–233. [CrossRef] [PubMed]

33. Zhang, W.; Liu, C.; Zheng, T.; Ma, J.; Zhang, G.; Ren, G.; Wang, L.; Liu, Y. Efficient oxidation and sorption of arsenite using a novel titanium(IV)-manganese(IV) binary oxide sorbent. *J. Hazard. Mater.* **2018**, *353*, 410–420. [CrossRef] [PubMed]

34. Nasrullah, A.; Khan, A.S.; Bhat, A.H.; Din, I.U.; Inayat, A.; Muhammad, N.; Bakhsh, E.M.; Khan, S.B. Effect of short time ball milling on physicochemical and adsorption performance of activated carbon prepared from mangosteen peel waste. *Renew. Energy* **2020**, *168*, 723–733. [CrossRef]

35. Chenglong, Z.; Zhiwei, X.; Fahui, N.; Kun, G.; Jiacheng, L. Application of hydroxyapatite-modified carbonized rice husk for the adsorption of Cr(VI) from aqueous solution. *J. Mol. Liq.* **2022**, *371*, 121137. [CrossRef]

36. Goldberg, S.; Johnston, C.T. Mechanisms of Arsenic Adsorption on Amorphous Oxides Evaluated Using Macroscopic Measurements, Vibrational Spectroscopy, and Surface Complexation Modeling. *J. Colloid Interface Sci.* **2001**, *234*, 204–216. [CrossRef] [PubMed]

37. Pierce, M.L.; Moore, C.B. Adsorption of arsenite and arsenate on amorphous iron hydroxide. *Water Res.* **1982**, *16*, 1247–1253. [CrossRef]

38. Liu, Z.; Chen, J.; Wu, Y.; Li, Y.; Zhao, J.; Na, P. Synthesis of magnetic orderly mesoporous α-Fe$_2$O$_3$ nanocluster derived from MIL-100(Fe) for rapid and efficient arsenic(III,V) removal. *J. Hazard. Mater.* **2017**, *343*, 304–314. [CrossRef] [PubMed]

39. Chen, J.; Wang, J.; Zhang, G.; Wu, Q.; Wang, D. Facile fabrication of nanostructured cerium-manganese binary oxide for enhanced arsenite removal from water. *Chem. Eng. J.* **2017**, *334*, 1518–1526. [CrossRef]

40. Zubair, Y.O.; Fuchida, S.; Tokoro, C. Insight into the Mechanism of Arsenic(III/V) Uptake on Mesoporous Zerovalent Iron–Magnetite Nanocomposites: Adsorption and Microscopic Studies. *ACS Appl. Mater. Interfaces* **2020**, *12*, 49755–49767. [CrossRef]